Hopping and trapping mechanisms in organic field-effect transistors

S. J. Konezny,* M. N. Bussac,† and L. Zuppiroli
Laboratoire d'Optoélectronique des Matériaux Moléculaires, STI-IMX-LOMM, Station 3, École Polytechnique Fédérale de Lausanne, CH-1015 Lausanne, Switzerland

(Received 28 April 2009; revised manuscript received 23 November 2009; published 15 January 2010)

A charge carrier in the channel of an organic field-effect transistor (OFET) is coupled to the electric polarization of the gate in the form of a surface Fröhlich polaron [N. Kirova and M. N. Bussac, Phys. Rev. B **68**, 235312 (2003)]. We study the effects of the dynamical field of polarization on both small-polaron hopping and trap-limited transport mechanisms. We present numerical calculations of polarization energies, band-narrowing effects due to polarization, hopping barriers, and interface trap depths in pentacene and rubrene transistors as functions of the dielectric constant of the gate insulator and demonstrate that a trap-and-release mechanism more appropriately describes transport in high-mobility OFETs. For mobilities on the order 0.1 cm^2/V s and below, all states are highly localized and hopping becomes the predominant mechanism.

DOI: 10.1103/PhysRevB.81.045313 PACS number(s): 72.80.Le, 71.38.Fp, 72.20.Jv

I. INTRODUCTION

Charge transport in single-crystal organic semiconductors is a difficult problem and many different models have been used to approach it.[1–5] For all of these models, the starting point are the transfer integrals acting in the crystal plane. The largest transfer integral J, which determines the bandwidth, is on the order of 100 meV. In addition to the fact that these systems have narrow bands, organic semiconductors are built with highly polarizable molecules and are subject to significant electron-phonon interactions. The carriers in organic semiconductors are therefore dressed with a lattice displacement cloud and an electrical polarization cloud.[6–9] In particular, recent scanning tunneling microscopy observations of site-specific polarization energies[8] give direct evidence of these electric polarization effects. Short-range lattice fluctuations and long-range polarization fluctuations must therefore be considered in transport models.[10] At room temperature, these fluctuations cause the dynamical localization of carriers,[4,11] which is reflected in the different power law dependence of the mobility versus temperature,[12,13] and versus transfer integral.[4] The weak localization length L determined by the transfer matrix method in two dimensions[4] typically varies from 50 lattice distances to 2 lattice distances for energetic disorder varying from $0.3J$ to $2J$.

Here we are interested in conduction processes that take place in the channel of an organic field-effect transistor built on an oxide or a polymer gate. Measurements of the charge carrier mobility in organic field-effect transistors (OFETs) are strongly dependent on the dielectric constant of the gate insulator.[9,14] These findings emphasize the importance of the coupling of the charge to the polarization of the nearby gate dielectric material.[15,16] In order to explain these results, we study the effects on the transport of the coupling of the carrier to the surface phonon modes of the gate insulator through its dielectric permittivity $\varepsilon(\omega)$. This situation is well described by a Fröhlich surface polaron Hamiltonian. Depending on the distance of the carrier to the gate interface and the nature of the dielectric, the coupling is either strong[15,17] or weak to moderate.[16] In the strong-coupling limit, the charge tends to form a small polaron,[17] whereas the carrier is less localized in the moderate coupling regime.[16]

In this paper, we discuss both trap-limited and small-polaron hopping transport mechanisms in the channel of an organic transistor close to gate interface. We present numerical calculations of these effects using pentacene and rubrene as model materials. For this purpose we numerically calculate the Coulomb polarization energy for free and localized or trapped states.[18] From these we deduce the activation energies for small-polaron hopping and for the trap-and-release process.

II. POLARIZATION ENERGY

A charge carrier in the bulk of an organic semiconductor polarizes the surrounding molecules and forms an electronic or Coulomb polaron[6,19] (see Fig. 1). For a carrier in the channel of an OFET (see Fig. 2), the charge polarizes the gate insulator in addition to the organic semiconductor. In both cases, the polarization energies E_p are on the order of 1 eV (see Table I).

Although E_p is large, Coulomb polaron formation is not, per se, an obstacle to charge propagation in the bulk of an organic semiconductor crystal. This is due to the fact that the polarization field induced by the charge establishes much

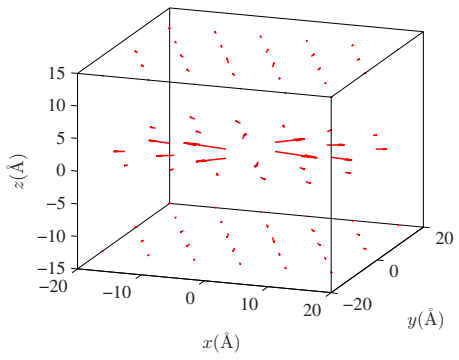

FIG. 1. (Color online) Coulomb polaron in bulk rubrene. The carrier is located at the origin in the $z=0$ high-mobility plane (a,b). The interlayer spacing is 13.4 Å.

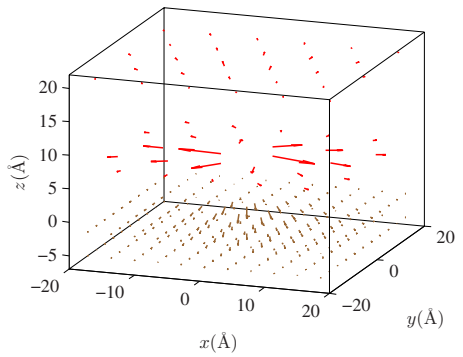

FIG. 2. (Color online) Induced cloud of polarization due to a hole in rubrene at $z=6.7$ Å close to a Ta_2O_5 interface at $z=0$. The induced dipoles in the oxide ($z<0$) are magnified by a factor of 5 relative to those in rubrene ($z>0$) for clarity.

faster than the time h/J required for its transfer to a neighboring molecular site, which is coupled to the initial site by a transfer integral J on the order of 100 meV. Thus the Bloch wave that forms in an organic solid is not that of a bare carrier but rather that of a carrier dressed with a cloud of electric polarization. Polarization effects do influence charge transport, however, since this coupling of the polarization field to the carrier in a Coulomb polaron leads to a larger effective mass[16] (see Tables III and IV).

Accurate calculations of the polarization energy are not straight forward because they involve long-range Coulomb potential contributions. The energy can, however, be calculated using a combination of numerical and analytical techniques that we have developed[4,16,18] as extensions to the self-consistent polarization field method.[6,20] One of two contributions to the polarization energy is calculated numerically, explicitly taking into account the anisotropy of the organic semiconductor polarizability and the dipole-dipole interactions in a cluster of molecules. The second contribution, which accounts for less than 10% of the total polarization energy, is analytically evaluated in the remaining region outside the cluster. An accurate result is achieved via a calibration procedure that ensures the polarization energy is independent of the size of the cluster for larger clusters. A more in-depth description of the calculation including details of the calibration procedure and tables of the parameters used in this work are given in Appendix A.

TABLE I. Electronic polarization energies in eV of a hole in rubrene and pentacene for the bulk case and in the organic semiconductor monolayer next to the semiconductor-insulator interface for common OFET gate insulators. The channel is 6.7 and 6.6 Å from the dielectric interface in rubrene and pentacene, respectively.

	Rubrene	Pentacene
Bulk	−0.834	−1.546
Vacuum	−0.776	−1.496
Parylene N	−0.860	−1.560
Parylene C	−0.863	−1.562
SiO_2	−0.842	−1.548
Al_2O_3	−0.873	−1.569
Ta_2O_5	−0.901	−1.589

III. CARRIER EFFECTIVE MASS EFFECTS AND COUPLING TO THE GATE INTERFACE

As a means of organizing the theoretical framework required to understand charge transport in high-mobility OFETs, it is instructive to discuss the timescales involved for each of the relevant charge interactions. A useful point of reference is the characteristic time it takes for Bloch-wave formation h/J, where J is the intermolecular charge transfer integral. The important interactions that occur on a timescale that is faster than Bloch-wave formation have the effect of reducing the effective transfer integral J^*, i.e. increasing the effective mass of the carrier $m^* \propto 1/J^*$. The two fast interactions that are relevant in the bulk of an organic semiconductor are molecular electric polarization and the coupling of the charge with high-frequency intramolecular phonon modes.[16] Slow interactions, on the other hand, act on the Bloch wave directly with the effect of localizing the charge. When localization effects are weak, as in the case of thermal fluctuations, the mobility is a power-law function of the renormalized transfer integral,[4]

$$\mu_0 \propto (J^*)^n, \tag{1}$$

where μ_0 is the mobility in the absence of traps and the exponent n is a material-specific value that can be deduced from temperature-dependent mobility data.[4] When self-trapping effects are strong, transport is interpreted in terms of small-polaron hopping.[17]

A. Polarization in the crystal bulk

The reduction in the transfer integral due to molecular polarization effects can be calculated by comparing the dipole fields surrounding a charge before and after propagation between two neighboring molecular sites n and $n+h$.[18] The dipoles induced by the charge are determined using the self-consistent polarization field method discussed in Sec. II and Appendix A. The reduction factor γ_p is defined as

$$\gamma_p = \exp(-S_0), \tag{2}$$

where

$$S_0(h) = \frac{1}{2}\sum_k \sum_{i=1}^{3} [X_{i,k}(n) - X_{i,k}(n+h)]^2, \tag{3}$$

$$X_{i,k} = \frac{d_{i,k}}{2\sqrt{e\alpha_{i,kk}}}, \tag{4}$$

$d_{i,k}$ and $\alpha_{i,kk}$ are the components of the induced dipole moment and polarizability tensor in the crystal basis of the organic molecule with index i, and e is the energy difference between the ground and first excited states of the neutral molecule.[16,18] The resulting factor by which the effective mass is increased due to molecular polarization effects γ_p^{-1} is 1.27 in bulk pentacene and 1.12 in bulk rubrene.

The coupling between the charge and the high-frequency intramolecular modes with frequencies $\hbar\omega_0$ that are larger than J/h gives rise to a narrowing of the effective bandwidth $4J^*$ by a factor of

$$\gamma_m = \exp(-E_m/\hbar\omega_0), \tag{5}$$

where E_m is the electron-phonon binding energy, i.e., 1/2 the reorganization energy of the molecule. The most significant contributions come from the 1343 and 1597 cm^{-1} vibrational modes in rubrene[25] and the 1441 and 1560 cm^{-1} modes in pentacene.[26,27] This gives rise to band narrowing in rubrene that is similar to the acenes. In both rubrene and pentacene the effective bandwidth is reduced by a factor of 0.75.

B. Polarization near a dielectric interface

In typical OFETs such as those based on rubrene and the acenes, the conductive channel is located in the organic semiconductor in proximity to the interface with the dielectric material. The presence of this interface gives rise to a coupling of the charge with the polarization of the dielectric material[15] and results in the formation of surface Fröhlich polarons. The coupling parameter α is related to the infrared-active surface phonon modes of the dielectric material with frequency $\hbar\omega_s$ and to the dielectric discontinuities at the interface in the following way:[16]

$$\alpha = \frac{q^2}{8\pi\varepsilon_0\varepsilon^* a\sqrt{\hbar\omega_s J'}}, \tag{6}$$

where

$$\frac{1}{\varepsilon^*} = \frac{\varepsilon_r - \varepsilon_\infty}{\varepsilon_r(\varepsilon_r + \varepsilon_\infty)} - \frac{\varepsilon_r - \varepsilon_s}{\varepsilon_r(\varepsilon_r + \varepsilon_s)}, \tag{7}$$

a in this case is the distance between two neighboring sites along the direction of charge propagation, ε_r is the effective dielectric constant of the organic semiconductor (Table V), ε_s and ε_∞ are the static and dynamic dielectric constants of the gate insulator (Table II), and $J' = \gamma_p\gamma_m J$ is the effective transfer integral including polarization and intramolecular-phonon effects.

Values of the surface phonon frequency $\omega_s = (\omega_L^2 + \omega_T^2)/2$, where ω_L and ω_T are the frequencies of the longitudinal and transverse optical phonons of the bulk oxide,[28] are given in Table II. The values of the coupling constants α are given in Tables III and IV. For a rubrene/Ta_2O_5 interface α=4.06, the relevant surface phonon energy is $\hbar\omega_s$=48.5 meV, and the renormalized transfer integral is J'=58 meV.

C. Strong coupling limit and small-polaron hopping

By using a method introduced by Pekar and Landau,[29,30] Kirova and Bussac presented a calculation for the surface Fröhlich polaron in the strong adiabatic coupling limit applied to the channel of an OFET. Similar results were used by Fratini *et al.* to justify the existence of small polarons in the channel of single-crystal rubrene transistors[14,17,31,32] that exhibited room-temperature mobilities as high as 20 cm^2/V s. Their model[32] was used to interpret the dependence of the mobility on both the temperature and the dielectric constant of the gate.[14]

TABLE II. Dielectric material parameters used in the model and literature values for rubrene OFET mobilities μ for various gate insulators. The values of the static ε_s and dynamic ε_∞ dielectric constants of the gate insulator were obtained from the same reference as the mobility data except for ε_∞ for parylene C, which was determined from Ref. 21. Values of the effective static α_s and dynamic α_∞ polarizabilities were calibrated using the procedure outlined in Sec. IV B of the text. Surface phonon frequencies ω_s for each dielectric material obtained and transverse and longitudinal phonon frequencies from the literature are also given.

	ε_s	α_s (Å^3)	ε_∞	α_∞ (Å^3)	ω_s (cm^{-1})	μ (cm^2/V s)
Vacuum	1	0	1	0		15–20[b]
Parylene N	2.9	4.21	2.56	3.74	500[b]	8–12[b]
Parylene C	3.15	4.53	2.65[c]	3.87	500[b]	6–10[a]
SiO_2	3.9	5.27	2.1	2.93	480[d]	4–7[b]
Al_2O_3	9.4	7.68	3	4.34	386[e]	2–4[b]
Ta_2O_5	25	9.04	4.4	5.67	390[f]	1–1.5[b]

[a]Reference 9.
[b]Reference 14.
[c]Reference 21.
[d]Reference 22.
[e]Reference 23.
[f]Reference 24.

D. Moderate coupling limit and the effective mass of the surface Fröhlich polaron

A careful study of the parameters that determine the existence of the surface Fröhlich polarons in rubrene transistors shows that $\hbar\omega_s/J' \approx 1$ and $\hbar\omega_s/k_BT \approx 2$ at room temperature, and that the characteristic distance of the channel to the gate interface $z/a \approx 1$. All of these values being on the order of one, the surface Fröhlich polaron cannot be consistently treated in either the strong or the weak coupling limit. This led to the introduction of a moderate coupling limit for polaron calculations in Ref. 16 (Appendix D) based on the ideas of Lee, Low, and Pines.[33] Here in Appendix B we reformulate this problem in a slightly simplified way where each molecule has no extension and can be considered simply a lattice node. The results compared to those in Ref. 16, where the extension of the molecules was considered, are the same within a few percent. In the moderate coupling limit, the polaron is large and its main effect is to increase the effective mass of the carrier.

The factor γ_s by which the effective transfer integral decreases due to surface polaron effects is determined via[16]

$$\frac{1}{\gamma_s} = 1 + 2\alpha\int_0^{\pi\sqrt{J'/\hbar\omega_s}} \frac{y^2}{(1+y^2)^3}\exp\left(-\frac{2yz}{a}\sqrt{\frac{\hbar\omega_s}{J'}}\right)dy. \tag{8}$$

The reduction factors and effective transfer integrals in the bulk and for various OFET interfaces for rubrene and penta-

TABLE III. Rubrene carrier bandwidth reduction factors due to molecular polarization γ_p, intramolecular charge vibration γ_m, and surface phonon coupling γ_s, resulting electron-phonon coupling constant α, renormalized transfer integral $J^*=\gamma_p\gamma_m\gamma_s J$ based on a reported[25] calculation of the bare transfer integral $J=85$ meV, calculated trap depth E_t of an interface defect with a dipole moment of 3.0 D, and mobility μ estimated using the model with an interface trap density of 1.8×10^{12} cm^{-2}.

	γ_p	γ_m	α	γ_s	J^* (meV)	E_t (meV)	μ (cm^2/V s)
Rubrene bulk	0.8893	0.75		1	56.69		
Rubrene/vacuum	0.8881	0.75		1	56.62		17.5
Rubrene/parylene N	0.8904	0.75	0.4015	0.9714	55.14	72.08	14.7
Rubrene/parylene C	0.8905	0.75	0.5551	0.9609	54.55	94.57	12.2
Rubrene/SiO_2	0.8900	0.75	2.016	0.8684	49.27	125.4	6.50
Rubrene/Al_2O_3	0.8907	0.75	3.640	0.7618	43.26	162.2	1.94
Rubrene/Ta_2O_5	0.8914	0.75	4.059	0.7425	42.19	168.4	1.52

cene are given in Tables III and IV. Values of $J^*=\gamma_s J'$ are based on calculations[25,34] of the bare transfer integral J in the absence of polarization and electron-phonon coupling effects.

IV. CHARGE TRANSPORT IN THE OFET CHANNEL

The models used to describe transport in the channel of an OFET typically involve either a trap-and-release mechanism[35,36] or small-polaron hopping.[17,31,32] We now examine both models in a manner that includes the effects of polarization discussed in the previous sections.

A. Polarization effects on small-polaron hopping

In a series of recent papers[17,31,32] charge transport in the channel of single-crystal organic field-effect transistors was attributed to small-polaron hopping and charge mobilities as high as 20 cm^2/V s were explained by invoking this mechanism.[17] The energy barrier Δ for small-polaron hopping was obtained by a fit of a standard hopping relation to experimental data, and the results were compared to a standard analytical hopping model. We now develop a numerical approach to get the value of the hopping barrier directly.

Textbook relations giving the mobility of small polarons usually derive from the Holstein's molecular-crystal model[37,38] or the Marcus theory of charge transfer.[39,40] We shall apply these models to the current problem of a polaron that occupies a molecule immersed in an electrically polarizable medium by making necessary corrections to the hopping frequency to account for long-range effects. For this small-polaron hopping model we consider a cluster of two adjacent hopping sites in proximity to the organic-dielectric interface of the transistor and therefore embedded in a heterogeneous electrically polarizable medium composed of the dielectric and the organic semiconductor. A single small polaron is on one of these two sites in the initial state and the hopping of the polaron occurs via a thermally assisted transition that is induced by thermal fluctuations of frequency ν.

When the temperature is high enough for atomic motion to be treated classically ($k_BT>h\nu/3$) the hopping rate becomes a thermally activated process. The polaron can make the hop in the presence of thermal fluctuations when the energies of the initial and final electronic states are coincident. The hopping activation energy is the minimum energy

TABLE IV. Pentacene carrier bandwidth reduction factors due to molecular polarization γ_p, intramolecular charge vibration γ_m, and surface phonon coupling γ_s, resulting electron-phonon coupling constant α, renormalized transfer integral $J^*=\gamma_p\gamma_m\gamma_s J$ based on a reported[34] calculation of the bare transfer integral $J=97.8$ meV, calculated trap depth E_t of an interface defect with a dipole moment of 3.0 D, and mobility reduction factor μ/μ_0 due to trapping effects estimated using the model with an interface trap density of 1.8×10^{12} cm^{-2}.

	γ_p	γ_m	α	γ_s	J^* (meV)	E_t (meV)	μ/μ_0
Pentacene bulk	0.7865	0.75		1	57.69		
Pentacene/vacuum	0.7781	0.75		1	57.07		1
Pentacene/parylene N	0.7800	0.75	0.4012	0.9812	56.14	121.1	0.4764
Pentacene/parylene C	0.7801	0.75	0.5598	0.9740	55.73	124.9	0.4353
Pentacene/SiO_2	0.7797	0.75	2.030	0.9092	52.00	158.7	0.1550
Pentacene/Al_2O_3	0.7803	0.75	4.003	0.8123	46.49	190.7	0.0426
Pentacene/Ta_2O_5	0.7808	0.75	4.799	0.7843	44.92	201.4	0.0272

required to achieve such a coincidence configuration.[37] This semiclassical hopping model is adiabatic if the lifetime h/J of the coincidence state (or charge transfer state) is shorter than the characteristic time $1/\nu$ of the fluctuation inducing the hop, or $h\nu < J$. Note that in the present case in which the carrier can be described as a Fröhlich polaron, the coincidence is mediated by long-range polarization effects.

The dielectric response of the bound charges in the oxide affects the hopping rate between two sites situated at the gate interface. This effect can be understood qualitatively by separating the polarizability of the oxide into two components: a fast electronic component related to the dielectric response α_∞ and a slow component for frequencies lower than J/h related to atomic motions in the dielectric response $\alpha' = \alpha_s - \alpha_\infty$. The fast component of the induced dipole field does not contribute to the hopping barrier since, as we emphasized in Sec. II, the time scales related to electronic redistribution both in the oxide and in the organic semiconductor in this case are much shorter than any other time scale of the interactions involved. This fast component increases the effective mass of the carrier when it tunnels across the barrier. This is accounted for by replacing the bare transfer integral J by its renormalized value J^* (see Sec. III).

There are two ways to envisage small polaron hopping in a cluster embedded in an electrically polarizable medium: the Holstein molecular model and the Marcus charge-transfer model, which, in this case, are not equivalent. In the view resulting from Emin-Holstein hopping theory, the slow dipoles of the oxide, which are at the origin of the surface polaron, are also responsible for the coincidence configuration and the hopping. In this case, the semiclassical calculation in the continuous limit has been reviewed by Fratini *et al.* in Ref. 31. The hopping barrier is

$$\Delta = \gamma E_{\mathrm{sp}} - t', \tag{9}$$

where $\gamma E_{\mathrm{sp}} = E_{\mathrm{sp}}(1) - E_{\mathrm{sp}}(2)$ and $E_{\mathrm{sp}}(1)$ and $E_{\mathrm{sp}}(2)$ are the surface polaron energies of the small-polaron and coincidence states, respectively.[41] The surface polaron energy is the sum of the polarization energy and the interaction energy between the charge and the induced dipoles. In the continuous limit it is equal to the interaction energy between the carrier and its image charge,[28]

$$E_{\mathrm{sp}} = \frac{q^2}{8\pi\varepsilon_0}\frac{\beta}{z}, \tag{10}$$

where $\beta = 1/2\varepsilon^*$ is defined in Eq. (7) and

$$\gamma = \frac{1}{2}\left(1 - \frac{z}{\sqrt{z^2 + a^2}}\right). \tag{11}$$

Here t' takes a value on the order of J^*.

In the case of the rubrene/Ta_2O_5 interface $\beta = 0.099$, $z = 6.7$ Å, $a = 7.2$ Å, the polaron binding energy $E_{\mathrm{sp}} = 107$ meV, and $\gamma = 0.16$. Based on these parameters, the hopping barrier $\Delta = 17$ meV$-t'$ is small. We know from Ref. 16 that there are significant differences between the discrete image force and the continuous one. Since this model is continuous and based on a classical image force dependence at the interface, we have computed the discrete equivalent.

Our discrete results for the rubrene/Al_2O_3 interface yield a polaron formation energy of 71 meV and a polaron hopping barrier of only 5 meV. Both the continuous and discrete results are very different from the fits of Fratini *et al.* to the experimental data that give $\Delta = 55$ meV for the rubrene/Ta_2O_5 interface and $\Delta = 47$ meV for the rubrene/Al_2O_3 interface. Taking a channel closer to the interface ($z = 3$ Å instead of $z = 6.7$ Å) will not increase the activation energy sufficiently ($\Delta = 32$ meV$-t'$ instead of $\Delta = 17$ meV$-t'$).

If we refer to the Marcus theory of charge transfer in a polarizable medium,[39,40] we can find a different way to calculate the activation energy Δ. This view is applicable when the charge is not only coupled to the slow dipoles of the oxide, but also to the other degrees of freedom that ensure coincidence. The polaron is built by the coupling of the carrier with the slow dipoles of the oxide and the coincidence results from other molecular fluctuations.

Immediately after the carrier makes the transition from the ground state to the coincidence state, the slow dipoles that were induced in the long-lived ground state due to the slow dielectric response α' have had no time to reorganize. The field of the carrier involved in the hop changes from the field of a point charge to the field of a charge split between two sites. Thus the charge transfer or small-polaron hopping barrier is written:

$$\Delta E = \frac{q}{4\pi\varepsilon_0}\sum_i \left[\frac{1}{2}\left(\frac{\mathbf{x}_i - \mathbf{a}}{|\mathbf{x}_i - \mathbf{a}|^3} + \frac{\mathbf{x}_i}{|\mathbf{x}_i|^3}\right) - \frac{\mathbf{x}_i}{|\mathbf{x}_i|^3}\right] \cdot \mathbf{d}_i(\alpha'), \tag{12}$$

where 0 and $\mathbf{a}$ are the locations of the two hopping sites, q is the charge of the carrier, and $\mathbf{d}_i(\alpha')$ are the dipoles induced on site i by the hopping carrier on the site at 0 due to the slow response. Equation (12) reflects the point emphasized by Marcus[39,40] that only a non-equilibrium dipole distribution [such as $\mathbf{d}_i(\alpha')$] can influence hopping.

We used the numerical procedure discussed in Appendix A to calculate the dipole field $\mathbf{d}_i(\alpha')$, which depends on the details of the geometry and dielectric response, for rubrene and pentacene transistors with various gate dielectrics. The corresponding small-polaron hopping barriers associated with these devices are plotted in Fig. 3 as a function of the static dielectric constant of the gate insulator. In a rubrene transistor with a Ta_2O_5 oxide gate, we find a hopping barrier of 12.4 meV. As in the continuous and discrete calculations above that we determined using the Holstein framework, this value is also much lower than the hopping barrier of 55 meV found by Fratini *et al.*[14,17,31,32]

In conclusion, the three different models that we used to describe small-polaron hopping ("continuous Holstein," "discrete Holstein," and "discrete Marcus" models) do not agree with the experimental results obtained in single-crystal rubrene OFETs. In all three cases, the hopping barriers are too small compared to k_BT and also too small with respect to the measured values. This suggests that the Fröhlich surface polaron is not a small polaron and favors the model presented in Appendix B (moderate coupling limit). This also motivates the study of transport processes other than hopping

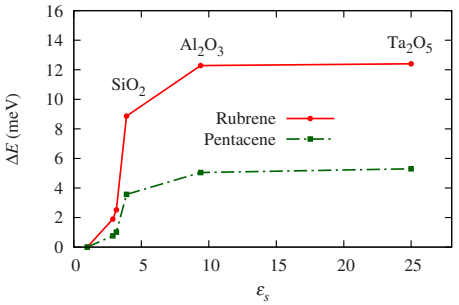

FIG. 3. (Color online) Dependence of the hopping energy of a hypothetical small polaron in the channel of a single-crystal OFET as a function of the dielectric constant of the gate dielectric. The calculation has been done according to Eq. (12) (Marcus theory of charge transfer in an electrically polarizable medium). The distance from the channel to the dielectric interface is 6.7 Å in rubrene and 6.6 Å in pentacene.

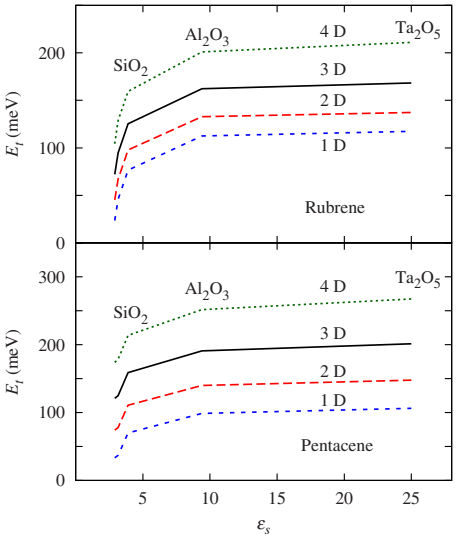

FIG. 4. (Color online) Hole trap depth in rubrene and pentacene transistors due to an interface defect dipole as a function of the static dielectric constant of the gate insulator for various dipole strengths from 1 to 4 debyes (D).

that are more sensitive to the value of the dielectric constant of the gate such as the trap-and-release model described in the following section.

B. Polarization effects on trap-limited transport

Treatments of the dielectric surface, such as plasma treatments or applications of self-assembled monolayers, prior to deposition of the organic semiconductor can greatly affect OFET performance.[42–44] This can be attributed to the difficulty in creating a dielectric surface that is free of electroactive defects. A "pristine" SiO_2 surface, for example, contains high concentrations of natural defects, peroxide bridges, free radicals, OH groups, and nonbridging oxygen centers, regardless of the steps taken to reduce their numbers.[45–47] These defects are expected to have or lead to dipole moments on the order of a few debye[48,49] that give rise to transport traps for carriers in the nearby channel of the transistor. This is consistent with interface trap density measurements that are between 1 and 3×10^{12} cm^{-2} in single-crystal rubrene-SiO_2 transistors,[50] two orders of magnitude higher than at the rubrene-vacuum interface in an air-gap transistor.[35]

As discussed in Sec. III, the fact that the organic semiconductors and oxide gates used in the OFETs of interest are polar materials means that a carrier in the channel will polarize its surroundings. The strength of this long-range Coulomb interaction can be greatly affected when the charge is near a permanent dipole at a defect site. The difference in polarization energy can be large enough, even at moderate dipole strengths, to trap the carrier and will depend on the polarizabilities of both the organic semiconductor and the dielectric material.

The trap depth E_t as it relates to the difference in polarization energy ΔE_p between the trapped and free states must be defined with careful consideration of the timescales involved. The trapped state of the charge is a long-lived state. Calculation of the polarization energy in this case therefore requires the static dielectric constant ε_s for the analytical solution and the static polarizability α_s for the numerical solution. It is also important to make the appropriate corrections to the polarization energy that take into account the lattice relaxation energy E_ℓ, which is on the order of 0.1 eV.[6] For the short-lived transport or transfer states associated with the free state of the carrier, ε_∞ and α_∞ are more appropriate and the lattice relaxation corrections do not apply. The difference between the polarization energy of the charge alone $E_{p,q}$ in a short-lived state and the polarization energy of the charge interacting with the dipole trap $E_{p,q+d}$ in a long-lived state is then

$$\Delta E_p = E_{p,q}(\varepsilon_\infty, \alpha_\infty) - E_{p,q+d}(\varepsilon_s, \alpha_s), \tag{13}$$

and the trap depth E_t calculated with respect to the edge of the band is

$$E_t = \Delta E_p + E_\ell - 2J^*. \tag{14}$$

Note that the last term in Eq. (14) is equal to half the renormalized bandwidth and accounts for the fact that E_p is measured from the center of the band. Values of the renormalized transfer integral J^* for holes in rubrene and pentacene that are based on the fast interaction reduction factors calculated in this work and bare transfer integral calculations reported by Bredas *et al.*[25,34] are given in Tables III and IV.

The trap depths due to an interfacial defect dipole in pentacene and rubrene OFETs are plotted in Fig. 4 as a function of ε_s for various dipole strengths. Note that for a dipole moment of a few debye, the trap depth is on the order of a few hundred meV and increases as a function of ε_s. This gives rise to a second contribution to the dependence of the carrier mobility on ε_s.

The mobility as a function of the trap concentration and depth can be determined using the expression of Hoesterey and Letson,[51]

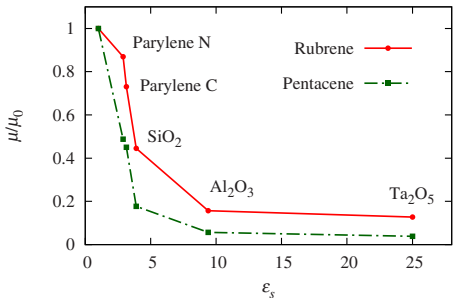

FIG. 5. (Color online) Mobility reduction factor μ/μ_0 due to trapping effects in the channel of rubrene and pentacene OFETs as a function of the gate insulator dielectric constant.

$$\mu = \frac{\mu_0(J^*)}{1 + c\,\exp(E_t/k_BT)}, \tag{15}$$

where $c=\sigma_t/\sigma$ is the relative trap concentration, σ_t is the surface trap density, σ is the surface density of the organic semiconductor, and μ_0 is the trap-free mobility.

As discussed in Sec. III B, the coupling strength between the charge and the polarization of the gate dielectric is in the weak to moderate range ($\alpha \lesssim 4$) and therefore Eq. (1) gives an accurate description of the trap-free mobility. This means that the dependence of the mobility on ε_s can be discussed in terms of coming from two contributions: effective mass effects on the trap-free mobility $\mu_0(J^*)$ and changes in the trap depth E_t as a function of ε_s. The effects of trapping alone can be seen in Fig. 5, which shows the mobility reduction factor μ/μ_0 for holes in rubrene and pentacene with a trap dipole of 3.0 D and a trap density of $\sigma_t=1.8\times10^{12}$ cm^{-2}, values that are consistent with the range of expected defect dipole moments[48,49] and reports of σ_t for rubrene/SiO_2 transistors.[50]

Measurements of the hole mobility in rubrene transistors reported in Refs. 9 and 14 are plotted as a function of ε_s in Fig. 6 with the trap-free and trap-limited mobilities calculated using the model and the parameters outlined in Tables III and V. The trap-free mobility is normalized to the mean experimental value of the rubrene air-gap transistor. Decreases in hole mobility due to increases in both the effective mass and the trap depth give rise to a strong decrease in $\mu(\varepsilon_s)$ that is in good agreement with experiment.

C. Trapping or hopping?

While both hopping and trap-and-release mechanisms may occur in devices that exhibit moderate carrier mobilities, a temperature-dependent upper bound $\mu_{max}(T)$ can be placed on the small-polaron hopping mobility.[52] This bound arises due to the fact that adiabatic hopping is always faster than nonadiabatic hopping and that the hopping rate reaches a maximum when the carrier interacts with the highest possible phonon energy $h\nu$ compatible with the hopping process. This energy is restricted by two conditions that we presented in Sec. IV A for adiabatic hopping, namely,

$$h\nu < J, \tag{16}$$

and

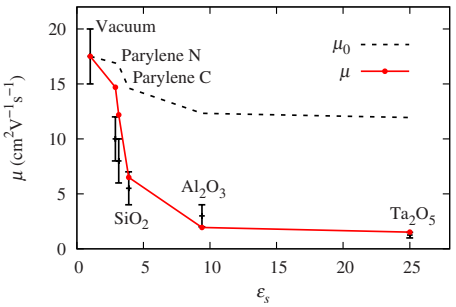

FIG. 6. (Color online) Trap-free mobility μ_0 and trap-controlled mobility μ as functions of the gate insulator dielectric constant shown with the ranges of experimental data reported in Refs. 9 and 14.

$$h\nu < 3k_BT. \tag{17}$$

In rubrene, which has an effective integral of $J^*=57$ meV (see Ref. 17 and Table III), the first condition corresponds to an upper limit of 500 cm^{-1} for ν. The relevant surface phonons presented in Table II fulfill this condition ($\nu=390$ cm^{-1} in Ta_2O_5).

The upper bound of the mobility can then be calculated using the following general assumptions. We begin with the Einstein relation for a nondegenerate carrier gas,

$$\mu(T) = qD/k_BT, \tag{18}$$

where D is the diffusion coefficient. We assume that, in the transport channel, the hopping motion is two dimensional, in which case $D=\gamma a^2/4$, where γ is the hopping rate and a is the hopping distance. The hopping rate takes the form of the product of the typical frequency of the phonon assisting the jump and the probability P to overcome the hopping barrier via a coincidence state. The upper bound of the mobility is obtained by assuming that each attempt to pass the barrier in the forward direction is successful ($P=1/2$), in which case

$$\mu_{max}(T) = q\nu a^2/8k_BT. \tag{19}$$

Using $a=7.2$ Å and $\nu=500$ cm^{-1}, the room-temperature mobility of small-polaron hopping in rubrene has an upper bound on the order of 0.4 cm^2/V s. Reports of the mobility in rubrene single-crystal OFETs are up to two orders of magnitude higher than this value,[14] which is consistent with the difficulties discussed in Sec. IV A of applying the small-polaron model to this data. In pentacene, μ_{max} would be even lower (0.2 cm^2/V s).

A plausible way in which the hopping process in an OFET channel can be made more sensitive to the dielectric response of the gate is to introduce more disorder, i.e., to consider energetically nonequivalent sites distributed over larger distances. This point was already discussed by Veres *et al.*, who observed large polarization effects in transistors with more disordered organic-gate interfaces and transistor mobilities on the order of 10^{-5} to 10^{-2} cm^2/V s.[53]

V. CONCLUSIONS

We studied the effects of polarization on both trap-and-release and small-polaron hopping transport in organic field-

effect transistors and found that a trap-and-release model is a better description when carrier mobilities are larger than approximately 0.1 cm^2/V s, while hopping transport can begin to be observed in OFETs exhibiting mobilities below this value.

We used a trap-limited transport model for high-mobility OFETs that includes the important effects of polarization and interface trapping to explain the experimental observations of large reductions in the carrier mobility with increasing static dielectric constant of the gate insulator ε_s.

We also calculated the trap depth of the interface defects that exist in typical OFETs using rubrene and pentacene transistors with various dielectric materials as examples. The difference in polarization energy between trapped and free states constitutes a large contribution to the trap depth that is dependent on ε_s. The combination of both the trap-free mobility and the interface trap depth being functions of ε_s gives rise to a trap-controlled mobility that rapidly decreases with increasing ε_s. Estimates of the carrier mobility in rubrene transistors for various dielectric materials are in good agreement with experimental data.

ACKNOWLEDGMENTS

This work was supported by the Swiss National Science Foundation (Project No. 200020-113254).

APPENDIX A: POLARIZATION ENERGY CALCULATIONS

The calculations of the polarization energy we used to determine the effects of polarization on the charge transport mechanisms in rubrene and pentacene were performed using the self-consistent polarization field method.[6] With this method all electrostatic interactions are explicitly taken into account within a finite region ρ containing the charge using the polarizability tensors and crystal structures of the surrounding polarizable media. An iterative procedure is used to calculate the induced dipole on each of the molecules within the region ρ due to: (i) the electric field $\mathbf{E}_1$ of the charge and, in the case of a trapped carrier, the permanent dipole of the proximate interface defect and (ii) the self-consistent field of the other induced dipoles.

In the channel of an OFET, the electric field for a charge q located at $\mathbf{x}_q$ that is trapped by an interface defect dipole $\mathbf{d}_t$ located at $\mathbf{x}_t$ is

$$\mathbf{E}_1(\mathbf{x}) = \frac{1}{4\pi\varepsilon_0}\left[q\frac{\mathbf{x}-\mathbf{x}_q}{|\mathbf{x}-\mathbf{x}_q|^3} - \frac{\mathbf{d}_t}{|\mathbf{x}-\mathbf{x}_t|^3} + 3(\mathbf{x}-\mathbf{x}_t)\frac{\mathbf{d}_t\cdot(\mathbf{x}-\mathbf{x}_t)}{|\mathbf{x}-\mathbf{x}_t|^5}\right]. \tag{A1}$$

The contribution of the polarization energy within the self-consistency region can be expressed in terms of the induced dipoles in the following way:

$$E_{\text{int}} = -\frac{q}{4\pi\varepsilon_0}\frac{(\mathbf{x}_t-\mathbf{x}_q)\cdot\mathbf{d}_t}{|\mathbf{x}_t-\mathbf{x}_q|^3} - \sum_i\left(\mathbf{E}_1(\mathbf{x}_i)\cdot\mathbf{d}_i - \sum_{k=1}^{3}\frac{(d_{i,k})^2}{2\alpha_{i,kk}}\right.$$
$$\left. - \frac{1}{4\pi\varepsilon_0}\sum_{j>i}\left[\frac{\mathbf{d}_i\cdot\mathbf{d}_j}{|\mathbf{x}_i-\mathbf{x}_j|^3} - 3\mathbf{d}_i\cdot(\mathbf{x}_i-\mathbf{x}_j)\frac{\mathbf{d}_j\cdot(\mathbf{x}_i-\mathbf{x}_j)}{|\mathbf{x}_i-\mathbf{x}_j|^5}\right]\right), \tag{A2}$$

where the position and induced dipole moment of the molecule with index i are denoted by $\mathbf{x}_i$ and $\mathbf{d}_i$, respectively. For the summation over the index i, which like j includes all organic semiconductor and gate dielectric molecules, only the first term in Eq. (A1) is used when $\mathbf{x}_i=\mathbf{x}_t$ and the electric field $\mathbf{E}_1$ is zero when $\mathbf{x}_i=\mathbf{x}_q$. The first term in Eq. (A2) is the charge-dipole interaction between the point charge and the permanent dipole of the trap. The remaining terms are the charge-dipole interactions, self-energies, and dipole-dipole interactions of the induced dipoles. As an example result of the numerical procedure, Fig. 7 shows some of the induced dipoles in a single-crystal rubrene channel due to a hole that has been trapped by a SiO_2 surface defect with a dipole strength of 2.0D. For a free carrier, E_{int} is calculated using the same procedure with all terms containing $\mathbf{x}_t$ removed from Eqs. (A1) and (A2).

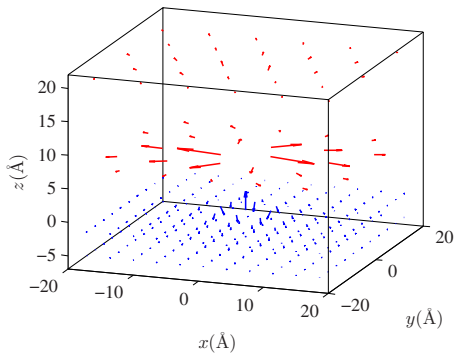

FIG. 7. (Color online) Hole trapped by an SiO_2 interface defect with a dipole moment of 2.0 D. The induced dipoles in rubrene ($z>0$) are shown for the first two monolayers adjacent to the interface located at $z=0$. For clarity, the strength of the dipoles in the region $z<0$ is magnified by a factor of 5 relative to those in rubrene.

Outside the self-consistency region, the remaining contribution of the polarization energy E_{ext} is estimated analytically using the macroscopic approximation that the dielectric constants of the media are isotropic. The isotropic dielectric constants reported in the literature for the gate dielectrics studied in this work are listed in Table II. The relevant gate insulator dielectric constant (ε_s or ε_∞) to be used in the calculation is determined by the timescale of the mechanism involved (see Sec. IV). We assumed that the static and dynamic dielectric constants in the organic semiconductor are identical and determined effective values based on reported anisotropic refractive indices in rubrene[56] and anisotropic dielectric tensor components in pentacene.[20] The effective dielectric constant ε_r of the organic semiconductor can be determined by the relation:[57]

$$\varepsilon_r = \frac{\sqrt{\varepsilon_2(\varepsilon_3-\varepsilon_1)}}{F\left(\arctan\sqrt{\frac{\varepsilon_3-\varepsilon_1}{\varepsilon_1}}, \sqrt{\frac{\varepsilon_3(\varepsilon_2-\varepsilon_1)}{\varepsilon_2(\varepsilon_3-\varepsilon_1)}}\right)}, \tag{A3}$$

where F is the elliptic integral of the first kind and ε_i are the principal components of the organic semiconductor dielectric tensor such that $\varepsilon_1>\varepsilon_2>\varepsilon_3$.

For accurate determination of the total polarization energy E_p, the microscopic molecular polarizability of the numerical solution inside ρ must be calibrated with respect to the mac-

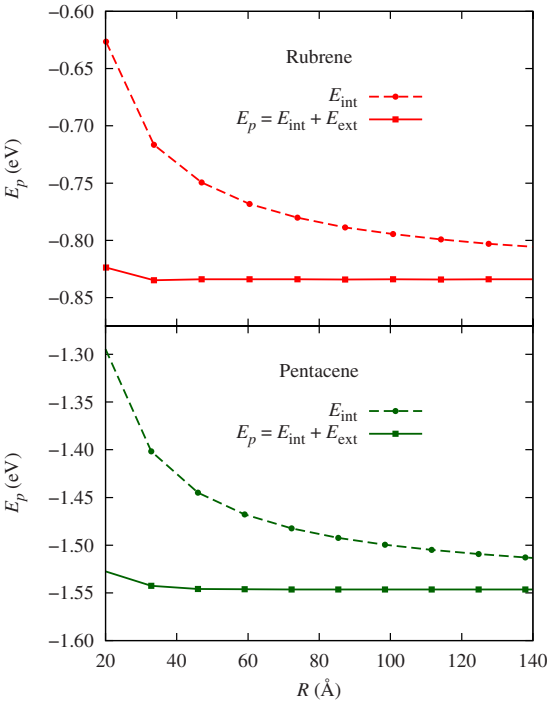

FIG. 8. (Color online) Numerical components of the polarization energy E_{int} inside a cylinder of radius R and height $2R$ and the total polarization energies E_p as functions of the cylinder radius for bulk rubrene and pentacene.

roscopic dielectric constant of the analytical solution outside ρ. This is achieved by adjusting the polarizability such that $E_p = E_{int} + E_{ext}$ is independent of the size of the self-consistency region for large ρ. To determine the polarization energy of a charge in proximity to a dielectric interface, it is convenient to use a cylindrical self-consistency region. It is worth noting that although Eq. (A3) was derived for the case in which ρ is a sphere,[57] we find calibrated polarizabilities and bulk polarization energies using a cylinder with radius R and height $2R$ that are identical to the results using a sphere within the sensitivity of the calculation.

The analytical component of the polarization energy of a trapped carrier is the solution to a boundary value problem that considers the dielectric discontinuity at the organic-dielectric interface and the resulting image charges. For a charge in the organic semiconductor located at located at $\mathbf{x} = a\hat{\mathbf{z}}$, a permanent dipole due to a defect in the gate dielectric centered at $\mathbf{x} = -b\hat{\mathbf{z}}$, and an organic-dielectric interface at the $z=0$ plane, the polarization energy in cylindrical coordinates is

$$E_{ext} = -\pi\varepsilon_0 \int\int (\varepsilon - 1)\mathbf{E}_0(\mathbf{x}) \cdot \mathbf{E}(\mathbf{x}) r dr dz, \tag{A4}$$

where

$$\varepsilon = \begin{cases} \varepsilon_r, & z > 0 \\ \varepsilon_s, & z \le 0 \end{cases}. \tag{A5}$$

The electric field of the charge and dipole in vacuum is

$$\mathbf{E}_0(\mathbf{x}) = \frac{q}{4\pi\varepsilon_0}\left[\frac{r\hat{\mathbf{r}} + (z+b+c)\hat{\mathbf{z}}}{\ell_{++}^3} - \frac{r\hat{\mathbf{r}} + (z+b-c)\hat{\mathbf{z}}}{\ell_{+-}^3} + \frac{r\hat{\mathbf{r}} + (z-a)\hat{\mathbf{z}}}{\ell_{-}^3}\right]. \tag{A6}$$

Note that we have assumed that the field is evaluated at a great enough distance so that the permanent dipole of the interface defect with strength μ_D can be treated as two charges separated by a distance of $2c = \mu_D / q$. This assumption is valid for our results because c is at least two orders of magnitude smaller than $|\mathbf{x}|$ for dipole strengths of a few debye and the sizes of ρ used.

The field in the dielectric media can be defined as

$$\mathbf{E}(\mathbf{x}) = \begin{cases} \mathbf{E}_+(\mathbf{x}), & z > 0 \\ \mathbf{E}_-(\mathbf{x}), & z \le 0 \end{cases}, \tag{A7}$$

where $\mathbf{E}_+(\mathbf{x})$ and $\mathbf{E}_-(\mathbf{x})$, given below, are the fields above and below the dielectric discontinuity, respectively. In the organic semiconductor, the electric field is

$$\mathbf{E}_+(\mathbf{x}) = \frac{q}{4\pi\varepsilon_r\varepsilon_0}\left\{\left(\frac{\varepsilon_r - \varepsilon_s}{\varepsilon_r + \varepsilon_s}\right)\frac{r\hat{\mathbf{r}} + (z+a)\hat{\mathbf{z}}}{\ell_+^3} + \left(\frac{2\varepsilon_r}{\varepsilon_r + \varepsilon_s}\right) \times \left[\frac{r\hat{\mathbf{r}} + (z+b+c)\hat{\mathbf{z}}}{\ell_{++}^3} - \frac{r\hat{\mathbf{r}} + (z+b-c)\hat{\mathbf{z}}}{\ell_{+-}^3}\right] + \frac{r\hat{\mathbf{r}} + (z-a)\hat{\mathbf{z}}}{\ell_-^3}\right\}, \tag{A8}$$

where

$$\ell_\pm = \sqrt{r^2 + (z \pm a)^2}, \tag{A9}$$

and

$$\ell_{\pm\pm} = \sqrt{r^2 + (z \pm b \pm c)^2}. \tag{A10}$$

In the gate dielectric, the field is

$$\mathbf{E}_-(\mathbf{x}) = \frac{q}{4\pi\varepsilon_s\varepsilon_0}\left\{\left(\frac{2\varepsilon_s}{\varepsilon_s + \varepsilon_r}\right)\frac{r\hat{\mathbf{r}} + (z-a)\hat{\mathbf{z}}}{\ell_-^3} + \left(\frac{\varepsilon_s - \varepsilon_r}{\varepsilon_s + \varepsilon_r}\right) \times \left[\frac{r\hat{\mathbf{r}} + (z-b-c)\hat{\mathbf{z}}}{\ell_{--}^3} - \frac{r\hat{\mathbf{r}} + (z-b+c)\hat{\mathbf{z}}}{\ell_{-+}^3}\right] - \frac{r\hat{\mathbf{r}} + (z+b+c)\hat{\mathbf{z}}}{\ell_{++}^3} + \frac{r\hat{\mathbf{r}} + (z-b+c)\hat{\mathbf{z}}}{\ell_{-+}^3}\right\}. \tag{A11}$$

For calculations of the polarization energy of a free carrier, the same analytical expressions above are used except that all terms containing b are removed and ε_s is replaced by ε_∞.

Fig. 8 shows the polarization energies of a hole in bulk rubrene and pentacene as functions of R for the calibrated values of the organic semiconductor polarizabilities given in Table V. As in all calculations of E_p, γ_p, and E_t presented in this work, the height of the cylindrical self-consistency region is equal to $2R$. The variation in the polarization energy is less than 0.3 meV for $R \gtrsim 60$ Å. Based on these results, dimensions of ρ for calculations of γ_p and E_t were chosen such that $R \approx 60$ Å. For calculations of γ_p in bulk rubrene and bulk pentacene, for example, a cylinder height equal to

TABLE V. Organic semiconductor parameters used in the model. Crystal lattice and molecular orientation constants and dielectric tensor principal components were obtained from the literature. The effective dielectric constants ε_r were determined using Eq. (A3) and the calibration procedure for obtaining the anisotropic polarizability components α_{ii} is outlined in Sec. IV B of the text.

	Rubrene	Pentacene
a,b,c(Å)	7.193, 14.433, 26.86[b]	7.9, 6.06, 16.01[c]
α,β,γ(°)	90, 90, 90	101.9, 112.6, 85.8[c]
$\varepsilon_a,\varepsilon_b,\varepsilon_c$	2.3, 2.6, 3.1[d]	5.336, 3.211, 2.413[a]
ε_r	2.62	3.58
$\alpha_{11},\alpha_{22},\alpha_{22}$(Å^3)	54.48, 43.55, 35.90	33.18, 23.03, 14.27

[a]Reference 20.
[b]Reference 54.
[c]Reference 55.
[d]Reference 56.

nine monolayers of the organic semiconductor was chosen.

A similar calibration technique was used to determine the isotropic polarizability for the gate dielectric molecules in a simple cubic geometry as a function of the dielectric constant. Results of this calibration for the static and dynamic dielectric constants relevant to the gate insulators studied are presented in Table II.

APPENDIX B: THE FRÖHLICH SURFACE POLARON

When a charge carrier is generated by the field effect at the interface between a molecular semiconductor and a gate insulator, it interacts with the surface phonons of the dielectric. This effect has been studied in Ref. 33 for an isotropic three-dimensional molecular crystal in the adiabatic limit. Here, we consider this interaction in the case of a crystal in which the carrier motion is essentially two dimensional and the electron-phonon coupling is moderate.

The electron-phonon interaction involving a charge in a particular monolayer of the crystal at a distance $z>0$ from the interface is given by[15]

$$H_{\text{e-ph}} = \sum_k \frac{q}{\sqrt{k}} \sqrt{\frac{\pi\hbar\omega_s}{S\varepsilon^*}} \sum_n e^{-kz} e^{i\mathbf{k}\cdot\mathbf{n}a} (b_k + b_{-k}^+) |\psi_n|^2, \tag{B1}$$

where $|\psi_n|^2$ is the charge density at site $\mathbf{n}a=(n_x a, n_y a)$, b_k and b_{-k}^+ are the annihilation and creation operators of the surface phonons in the gate dielectric, ω_s is the surface phonon frequency, and S is the surface area of the interface. The total Hamiltonian is then

$$H = -J' a^2 \frac{p^2}{\hbar^2} + \sum_k \hbar\omega_s b_k^+ b_k + H_{\text{e-ph}}, \tag{B2}$$

where $\mathbf{p}$ is the charge carrier momentum. Following Ref. 33, we introduce the total momentum of the system, which is a constant of motion in the total Hamiltonian,

$$\mathbf{P} = \sum_k \hbar\mathbf{k} b_k^+ b_k + \mathbf{p}. \tag{B3}$$

The total Hamiltonian can be transformed from H to H' through the unitary transformation $\hat{S}$ so that H' no longer contains the charge coordinates,

$$H' = \hat{S}^{-1} H \hat{S}, \tag{B4}$$

with

$$\hat{S} = \exp\left[i\left(\mathbf{P} - \sum_k b_k^+ b_k \mathbf{k} \right) \cdot \mathbf{n}a \right]. \tag{B5}$$

We therefore obtain

$$H' = \sum_k \hbar\omega_s b_k^+ b_k + \sum_k V_k(z)(b_k + b_{-k}^+) \left[\mathbf{P}/\hbar - \sum_k b_k^+ b_k k \right] J' a + \left[\mathbf{P}/\hbar - \sum_k b_k^+ b_k \right] J' a^2, \tag{B6}$$

where

$$V_k(z) = \frac{q}{\sqrt{k}} \sqrt{\frac{\pi\hbar\omega_s}{S\varepsilon^*}} e^{-kz}. \tag{B7}$$

Since the phonon frequency $\hbar\omega_s$ is comparable to the effective transfer integral J', the adiabatic approximation is not applicable. However, in our case, the dimensionless parameter α_{eff}, which describes the strength of the electron-phonon coupling and decreases as a function of the distance z to the interface as

$$\alpha_{\text{eff}} = \frac{q^2}{8\pi\varepsilon_0\varepsilon^* z} \equiv \alpha \frac{a}{z}, \tag{B8}$$

is on the order of 1 for a charge carrier located in the first monolayer.

We then use a variational method to describe the interaction of the dressed charge carrier with the dielectric phonons.[33] Introducing a second unitary transformation,

$$\hat{U} = \exp\left(\sum_k b_k^+ f_k - b_k f_k^* \right), \tag{B9}$$

where f_k is chosen to minimize the energy,

$$E = \frac{\mathbf{P}^2}{\hbar} a^2 J' + \sum_k (V_k f_k - V_k^* f_k^*) + J' \left(\sum_k |f_k|^2 k^2 a^2 \right)^2 + \sum_k |f_k|^2 \left[\hbar\omega_s + J' \left(k^2 a^2 - 2 \frac{\mathbf{k}\cdot\mathbf{P}}{\hbar^2} a^2 \right) \right], \tag{B10}$$

we then find

$$f_k = -\frac{V_k^*}{\hbar\omega_s + J'} \left[k^2 a^2 - 2 \frac{\mathbf{k}\cdot\mathbf{P}}{\hbar} a^2 (1-\eta) \right], \tag{B11}$$

where η satisfies the implicit equation,

$$\eta\mathbf{P} = \frac{\Sigma_k |V_k|^2 \hbar\mathbf{k}}{\hbar\omega_s + J'[k^2 a^2 - 2\mathbf{k}\cdot\mathbf{P}(1-\eta)a^2/\hbar]}. \tag{B12}$$

The carrier binding energy is $E_b = -\alpha I_1(z)\hbar\omega_s$ and the effective mass is $m^*/m = J'/J^* = 1 + 2\alpha I_2(z)$. As long as

$J'P^2a^2/\hbar^2$ is small ($\lesssim\hbar\omega_s$), we may obtain $E(P^2)$ to first order in an expansion of powers of $(J'/\hbar\omega_s)(P^2a^2/\hbar^2)$. In doing so, one readily gets

$$E = -\alpha I_1(z)\hbar\omega_s + \frac{P^2a^2}{\hbar^2}\frac{J'}{[1+2\alpha I_2(z)]}, \tag{B13}$$

where

$$I_1(z) = \int_0^{\pi\sqrt{J'/\hbar\omega_s}} \frac{1}{1+y^2}\exp\left(-\frac{2yz}{a}\sqrt{\frac{\hbar\omega_s}{J'}}\right)dy, \tag{B14}$$

and

$$I_2(z) = \int_0^{\pi\sqrt{J'/\hbar\omega_s}} \frac{y^2}{(1+y^2)^3}\exp\left(-\frac{2yz}{a}\sqrt{\frac{\hbar\omega_s}{J'}}\right)dy. \tag{B15}$$

*Present address: Department of Chemistry, Yale University, P.O. Box 208107, New Haven, CT 06520-8107, USA; sjkonezny@gmail.com

†Permanent address: Centre de Physique Théorique, UMR-7644 du Centre National de la Recherche Scientifique, École Polytechnique, F-91128 Palaiseau Cedex, France.

[1] A. Troisi, Adv. Mater. **19**, 2000 (2007).
[2] K. Hannewald and P. A. Bobbert, Phys. Rev. B **69**, 075212 (2004).
[3] K. Hannewald and P. A. Bobbert, Appl. Phys. Lett. **85**, 1535 (2004).
[4] J. D. Picon, M. N. Bussac, and L. Zuppiroli, Phys. Rev. B **75**, 235106 (2007).
[5] M. Unge and S. Stafstrom, Phys. Rev. B **74**, 235403 (2006).
[6] E. A. Silinsh and V. Capek, *Organic Molecular Crystals: Interacton Localization, and Transport Phenomena* (AIP Press, New York, 1994).
[7] J. K. Song, S. Y. Han, I. H. Chu, J. H. Kim, S. K. Kim, S. A. Lyapustina, S. J. Xu, J. M. Nilles, and K. H. Bowen, J. Chem. Phys. **116**, 4477 (2002).
[8] S. Soubatch, C. Weiss, R. Temirov, and F. S. Tautz, Phys. Rev. Lett. **102**, 177405 (2009).
[9] A. F. Stassen, R. W. I. de Boer, N. N. Iosad, and A. F. Morpurgo, Appl. Phys. Lett. **85**, 3899 (2004).
[10] P. Gosar and S. I. Choi, Phys. Rev. **150**, 529 (1966).
[11] A. Troisi and G. Orlandi, Phys. Rev. Lett. **96**, 086601 (2006).
[12] N. Karl, K. H. Kraft, J. Marktanner, M. Munch, F. Schatz, R. Stehle, and H. M. Uhde, J. Vac. Sci. Technol. A **17**, 2318 (1999).
[13] N. Karl, Synth. Met. **133-134**, 649 (2003).
[14] I. N. Hulea, S. Fratini, H. Xie, C. L. Mulder, N. N. Iossad, G. Rastelli, S. Ciuchi, and A. F. Morpurgo, Nature Mater. **5**, 982 (2006).
[15] N. Kirova and M. N. Bussac, Phys. Rev. B **68**, 235312 (2003).
[16] H. Houili, J. D. Picon, L. Zuppiroli, and M. N. Bussac, J. Appl. Phys. **100**, 023702 (2006).
[17] S. Fratini, A. F. Morpurgo, and S. Ciuchi, J. Phys. Chem. Solids **69**, 2195 (2008).
[18] M. N. Bussac, J. D. Picon, and L. Zuppiroli, Europhys. Lett. **66**, 392 (2004).
[19] Y. Toyozawa, Prog. Theor. Phys. **12**, 421 (1954).
[20] E. V. Tsiper and Z. G. Soos, Phys. Rev. B **68**, 085301 (2003).
[21] A. Kahouli, A. Sylvestre, L. Ortega, F. Jomni, B. Yangui, M. Maillard, B. Berge, J.-C. Robert, and J. Legrand, Appl. Phys. Lett. **94**, 152901 (2009).
[22] J. Humlicek and A. Roseler, Thin Solid Films **234**, 332 (1993).
[23] M. Schubert, T. E. Tiwald, and C. M. Herzinger, Phys. Rev. B **61**, 8187 (2000).
[24] E. Franke, C. L. Trimble, M. J. DeVries, J. A. Woollam, M. Schubert, and F. Frost, J. Appl. Phys. **88**, 5166 (2000).
[25] D. A. da Silva Filho, E. G. Kim, and J. L. Brédas, Adv. Mater. **17**, 1072 (2005).
[26] M. Malagoli, V. Coropceanu, D. A. da Silva, and J. L. Bredas, J. Chem. Phys. **120**, 7490 (2004).
[27] Note that in the case of rubrene, the timescales associated with couplings to the low-frequency modes, which have been assigned mainly to the bending of the phenyl side groups around the tetracene backbone of the molecule,[25] are too slow and therefore the contributions of the reorganization energy associated with these modes must be neglected in Eq. (5).
[28] J. Sak, Phys. Rev. B **6**, 3981 (1972).
[29] S. Pekar, Sov. Phys. JETP **16**, 335 (1946).
[30] S. Pekar, Sov. Phys. JETP **16**, 341 (1946).
[31] S. Fratini, H. Xie, I. N. Hulea, S. Ciuchi, and A. F. Morpurgo, New J. Phys. **10**, 033031 (2008).
[32] S. Ciuchi and S. Fratini, Phys. Rev. B **79**, 035113 (2009).
[33] T. D. Lee, F. E. Low, and D. Pines, Phys. Rev. **90**, 297 (1953).
[34] Y. C. Cheng, R. J. Silbey, D. A. da Silva, J. P. Calbert, J. Cornil, and J. L. Bredas, J. Chem. Phys. **118**, 3764 (2003).
[35] V. Podzorov, E. Menard, A. Borissov, V. Kiryukhin, J. A. Rogers, and M. E. Gershenson, Phys. Rev. Lett. **93**, 086602 (2004).
[36] W. L. Kalb, K. Mattenberger, and B. Batlogg, Phys. Rev. B **78**, 035334 (2008).
[37] D. Emin, Phys. Rev. Lett. **100**, 166602 (2008).
[38] T. Holstein, Ann. Phys. **8**, 343 (1959).
[39] R. A. Marcus, J. Chem. Phys. **24**, 979 (1956).
[40] R. A. Marcus, J. Phys. Chem. **98**, 7170 (1994).
[41] D. Emin, Phys. Rev. B **43**, 11720 (1991).
[42] M. Daraktchiev, A. von Muhlenen, F. Nuesch, M. Schaer, M. Brinkmann, M. N. Bussac, and L. Zuppiroli, New J. Phys. **7**, 133 (2005).
[43] A. von Mühlenen, M. Castellani, M. Schaer, and L. Zuppiroli, Phys. Status Solidi B **245**, 1170 (2008).
[44] M. Halik, H. Klauk, U. Zschieschang, G. Schmid, C. Dehm, M. Schutz, S. Maisch, F. Effenberger, M. Brunnbauer, and F. Stellacci, Nature (London) **431**, 963 (2004).
[45] V. Radzig, *Physico-Chemical Phenomena in Thin Films and at Solid Surfaces*, edited by S. H. L. Leonid, I. Trakhtenberg, and O. J. Ilegbusi (Academic Press, New York, 2007), Vol. 34, pp. 231–345.
[46] L. Giordano, P. V. Sushko, G. Pacchioni, and A. L. Shluger, Phys. Rev. B **75**, 024109 (2007).

[47] S. Suarez, F. D. Fleischli, M. Schaer, and L. Zuppiroli (unpublished).
[48] J. W. Raymonda, J. S. Muenter, and W. A. Klemperer, J. Chem. Phys. **52**, 3458 (1970).
[49] R. W. Fessenden, A. Hitachi, and V. Nagarajan, J. Phys. Chem. **88**, 107 (1984).
[50] C. Goldmann, C. Krellner, K. P. Pernstich, S. Haas, D. J. Gundlach, and B. Batlogg, J. Appl. Phys. **99**, 034507 (2006).
[51] D. C. Hoesterey and G. M. Letson, J. Phys. Chem. Solids **24**, 1609 (1963).
[52] I. G. Austin and N. F. Mott, Adv. Phys. **18**, 41 (1969).
[53] J. Veres, S. D. Ogier, S. W. Leeming, D. C. Cupertino, and S. M. Khaffaf, Adv. Funct. Mater. **13**, 199 (2003).
[54] O. D. Jurchescu, A. Meetsma, and T. T. M. Palstra, Acta Crystallogr., Sect. B: Struct. Sci. **62**, 330 (2006).
[55] R. B. Campbell, J. Trotter, and J. M. Robertson, Acta Crystallogr. **14**, 705 (1961).
[56] S. Tavazzi, A. Borghesi, A. Papagni, P. Spearman, L. Silvestri, A. Yassar, A. Camposeo, M. Polo, and D. Pisignano, Phys. Rev. B **75**, 245416 (2007).
[57] P. J. Bounds and R. W. Munn, Chem. Phys. **44**, 103 (1979).